

An analytical model of the scattered radiation distribution in diagnostic radiology

John M. Boone and J. Anthony Seibert

Citation: *Medical Physics* **15**, 721 (1988); doi: 10.1118/1.596186

View online: <http://dx.doi.org/10.1118/1.596186>

View Table of Contents: <http://scitation.aip.org/content/aapm/journal/medphys/15/5?ver=pdfcov>

Published by the [American Association of Physicists in Medicine](#)

Articles you may be interested in

[Monte Carlo simulation of the scattered radiation distribution in diagnostic radiology](#)

Med. Phys. **15**, 713 (1988); 10.1118/1.596185

[Scattered Radiation in Diagnostic Radiology by Bengt Nielsen](#)

Med. Phys. **14**, 426 (1987); 10.1118/1.596061

[Calculation of the smallangle distribution of scattered photons in diagnostic radiology using a Monte Carlo collision density estimator](#)


Med. Phys. **13**, 19 (1986); 10.1118/1.595933

[Physical characteristics of scattered radiation in diagnostic radiology: Monte Carlo simulation studies](#)

Med. Phys. **12**, 152 (1985); 10.1118/1.595771

[Coherent scatter in diagnostic radiology](#)


Med. Phys. **10**, 40 (1983); 10.1118/1.595443



Quality Reports™ with PlanIQ™

Prior to the start of plan design, see estimated achievability of the dose and DVH objectives based on the specific patient's anatomy.


- ✓ Objective and patient-specific analytics allow clinicians to create the best plan possible for each patient
- ✓ Equipping the treatment planner with more information earlier in the process enables a more efficient plan approval process for all
- ✓ Automation saves time and ensures that required reports are compliant



Free Live Webinar Series on Quality Reports with PlanIQ
sunuclear.com/webinars

Download the Quality Reports with PlanIQ Datasheet
sunuclear.com/QR

Your Most Valuable QA and Dosimetry Tools | sunuclear.com

 *Export only, 510(k) pending. Patent pending.

An analytical model of the scattered radiation distribution in diagnostic radiology

John M. Boone

Department of Radiology, Thomas Jefferson University, Philadelphia, Pennsylvania 19107

J. Anthony Seibert

Department of Radiology, University of California Davis Medical Center, Sacramento, California 95817

(Received 19 December 1986; accepted for publication 3 June 1988)

A simple scatter model is used to analytically derive the point spread function (PSF) for scattered radiation in diagnostic radiology. The resulting equation is a function of four physical parameters; object thickness, object-to-detector distance (air gap), and the linear attenuation coefficients for both primary and scatter radiation. Though the model is based upon single scattering, it is shown that by reducing the scatter attenuation coefficient the analytic model compares well to the multiple scattering PSF determined using Monte Carlo analysis.

I. INTRODUCTION

Scattered radiation can significantly deteriorate image quality in diagnostic radiology. Understanding the distribution and intensity of scattered radiation is an important step in designing techniques to reduce the detrimental effects of scatter on image quality. Computerized radiographic images have become more commonplace as that technology advances, and as a result many computer-based techniques for the correction of scattered radiation effects have emerged.¹⁻⁵ Common to many such techniques, is the requisite that the scatter point spread function be known. To illustrate this point in one class of computer-based scatter correction, deconvolution,^{1,3,5} the scatter point spread function (PSF) is used to mathematically determine a deconvolution filter. Though this approach is only an approximation, it is capable of significant contrast enhancement in many clinical situations. However, the scatter PSF is known to vary depending on the imaging geometry; specifically, the object thickness and object-to-detector distance (air gap) can have great effect on the shape and amplitude of the scatter PSF, as shown in a companion paper⁶ employing Monte Carlo techniques. Therefore, the ability to synthesize a scatter PSF based on the patient-specific imaging parameters would aid this approach and provide for a potentially robust scatter correction technique. We point out that scatter deconvolution is an experimental technique, and has its limitations.

In this paper, a single scatter approximation is derived for the scatter PSF in diagnostic radiology. The resultant equation is a function of four *physical* parameters; object thickness, air gap, and the linear attenuation coefficients for primary (μ_p) and scattered (μ_s) radiation. The first two parameters are clearly related to the object (or patient) being imaged, while the latter two are related to both the object being imaged and to the x-ray beam spectrum used. The model assumes a homogeneous object consisting of water-equivalent tissue, and thus inhomogeneities such as bone or gas are not considered. The PSF results will be compared with the PSF generated by Monte Carlo simulations, described in the previous companion article.

II. THEORY

Let the analytically derived scatter PSF be represented by $g(r)$. Radial symmetry exists because the probability of radial scattering at an angle ϕ is uniform from 0° to 360° .⁷ We integrate $g(r)$ over ϕ , and get the function $g'(r)$, where:

$$g'(r) = \int_{\phi=0}^{2\pi} g(r)r d\phi, \quad (1)$$

and thus

$$g(r) = (1/2\pi r)g'(r). \quad (2)$$

For the most part, we will deal with the modified scatter PSF, $g'(r)$, where $g'(r)$ is related to the scatter PSF $g(r)$ by Eq. (2). The reason for this is to decouple the relatively strong $1/2\pi r$ term, which can obscure the subtleties of the $g'(r)$ term. The (modified) PSF $g'(r)$ is derived assuming single scattering in a homogeneous scatter medium, separated from the detector by a uniform air gap. Spectral effects are not considered. Though the function derived is an approximation to the single scatter PSF, it may be applicable to the more general multiple scattering case through modification of the parameter μ_s . This will be discussed later. The terms used in the following discussion are defined in Fig. 1. Four components contribute to the function $g'(r)$: (1) the scatter source intensity, (2) the probability of scattering at a given angle, (3) scatter attenuation, and (4) the change in the detector cross section as a function of angle. These will be dealt with in order.

(1) The scatter cross section of a thin slab of homogeneous material (water) is the same regardless of its depth in the object, assuming negligible beam hardening. Since this probability is constant with depth, the resulting scatter intensity emitted from such a slab is proportional to the x-ray intensity incident on that slab. The intensity of scatter is proportional to the primary beam intensity at a depth $(t-s)$;

$$I_s = k_1 \exp[-\mu_p(t-s)], \quad (3)$$

where k_1 is a constant dealing with the incident primary

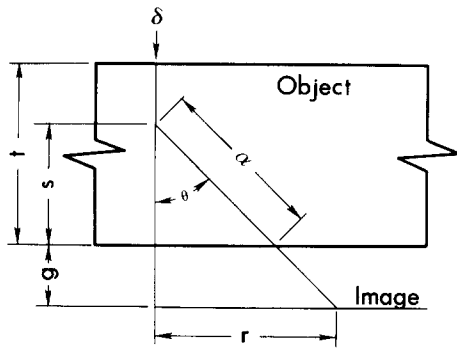


FIG. 1. The geometric setup used in deriving the analytic scatter PSF, $g'(r)$. Photons enter the object normally at δ . Object thickness: t ; air gap: g ; radial distance: r ; scatter angle: θ ; bottom of object to scatter focus: s ; path length of scatter through object: α .

intensity and μ_p is the effective linear attenuation coefficient of the primary beam.

(2) Assuming a small Rayleigh scattering component (discussed later), the collision cross section per solid angle is given by the Klein-Nishina formula:

$$\frac{d\sigma}{d\Omega} = k_2 \left(\frac{\nu}{\nu_0} \right)^2 \left(\frac{\nu}{\nu_0} + \frac{\nu_0}{\nu} - \sin^2 \theta \right), \quad (4)$$

where k_2 is a constant term⁷ and ν_0 and ν are the frequencies of the incident and scattered photons, respectively. The cross section as a function of scattering angle θ is found by substituting $d\Omega = 2\pi \sin \theta d\theta$;

$$\frac{d\sigma}{d\theta} = 2\pi k_2 \left(\frac{\nu}{\nu_0} \right)^2 \left(\frac{\nu}{\nu_0} + \frac{\nu_0}{\nu} - \sin^2 \theta \right) \sin \theta. \quad (5)$$

In diagnostic radiology, to a first approximation the loss in scattered photon energy and hence the change in frequency is small, such that $\nu \approx \nu_0$. For example, a 100-keV photon scattered at 45° loses only 5% of its energy. This simplification reduces Eq. (5) to

$$\frac{d\sigma}{d\theta} = 2\pi k_2 (2 \sin \theta - \sin^3 \theta). \quad (6)$$

(3) The scatter released at a given depth $(t - s)$ will transit a path length α through the object to reach the detector at a radial distance r . The attenuation due to this is given by

$$\text{attenuation} = \exp(-\mu_s \alpha), \quad (7)$$

where μ_s is the effective attenuation coefficient of scattered radiation, and:

$$\alpha = [s/(s+g)] [r^2 + (s+g)^2]^{1/2}.$$

(4) For a detector element dr at a distance r from the origin,

$$\frac{d\theta}{dr} = \frac{d}{dr} \tan^{-1} \left(\frac{r}{s+g} \right).$$

It is noted that $d\theta$ is used instead of the solid angle $d\Omega$ because the r axis represents the integrated annular area, as discussed earlier. This derivative yields:

$$\frac{d\theta}{dr} = \frac{1}{s+g} \left[1 + \left(\frac{r}{s+g} \right)^2 \right]^{-1}. \quad (8)$$

Combining Eqs. (3), (6), (7), and (8), and integrating over the thickness of the object, the scatter reaching a detector element at a distance r (integrated over ϕ) is

$$g'(r) = K \int_{s=0}^t \exp[-\mu_p(t-s)] \exp(-\mu_s \alpha) \\ \times (2 \sin \theta - \sin^3 \theta) \left(\frac{1}{s+g} \right) \left[1 + \left(\frac{r}{s+g} \right)^2 \right]^{-1} ds, \quad (9)$$

where K is a global constant encompassing several constant terms and

$$\theta = \tan^{-1} [r/(s+g)].$$

Note that Eq. (9) is a function of the object thickness t , the air gap g , and two attenuation coefficients μ_p and μ_s which relate to the quality of the beam. The utility of this equation when solved numerically will be discussed in detail in a later section.

Since the function $g'(r)$ represents the scatter PSF integrated over the radial axis, the area under $g'(r)$ corresponds to the total scattered energy. Therefore, the constant K is chosen such that the total area of $g'(r)$ is equal to the scatter-to-primary ratio (SPR_∞) for the particular object thickness and beam spectra. Thus:

$$\text{SPR}_\infty = \int_{r=0}^{\infty} g'(r) dr, \quad (10)$$

SPR_∞ is defined as the ratio of the scattered energy exiting the bottom surface of the object to the primary beam energy exiting the object. From this definition it is clear that SPR_∞ is independent of the air gap.

III. RESULTS

The functional form of $g'(r)$ is compared with the (modified) scatter PSF, $h'(r)$, determined using Monte Carlo (MC) simulation as described in the companion paper.⁶ The two functions, $g'(r)$ and $h'(r)$, are compared graphically in Figs. 2–5. In these figures, the functional dependency of $g'(r)$ and $h'(r)$ on both air gap and object thickness is shown. Each curve in these figures represents a different object thickness and air gap, and the appropriate values for both were used in the computation of $g'(r)$. The effective primary beam attenuation coefficient was calculated in the MC analysis and for the 100-kVp spectrum $\mu_p = 0.2184 \text{ cm}^{-1}$. Least-squares analysis over all 12 distributions (Figs. 2–5) resulted in a best-fit value of $\mu_s = 0.1328 \text{ cm}^{-1}$. The values $\mu_p = 0.2184$ and $\mu_s = 0.1328$ were used in all 12 curves shown in Figs. 2–5. Therefore, the differences in $g'(r)$ between the figures are solely the result of the thickness and air gap parameters, t and g . The result supports the appropriateness of the model used in developing $g'(r)$, and also demonstrates the utility of $g'(r)$ [i.e., Eq. (9)] in scatter PSF research applications. The values of μ_p and μ_s are specific to the x-ray spectrum, whereas t and g describe the geometrical configuration of the imaging procedure. The values of μ_p and μ_s for other x-ray spectra are given in Table I. The values of SPR_∞ , required to normalize the strength of the PSF, are

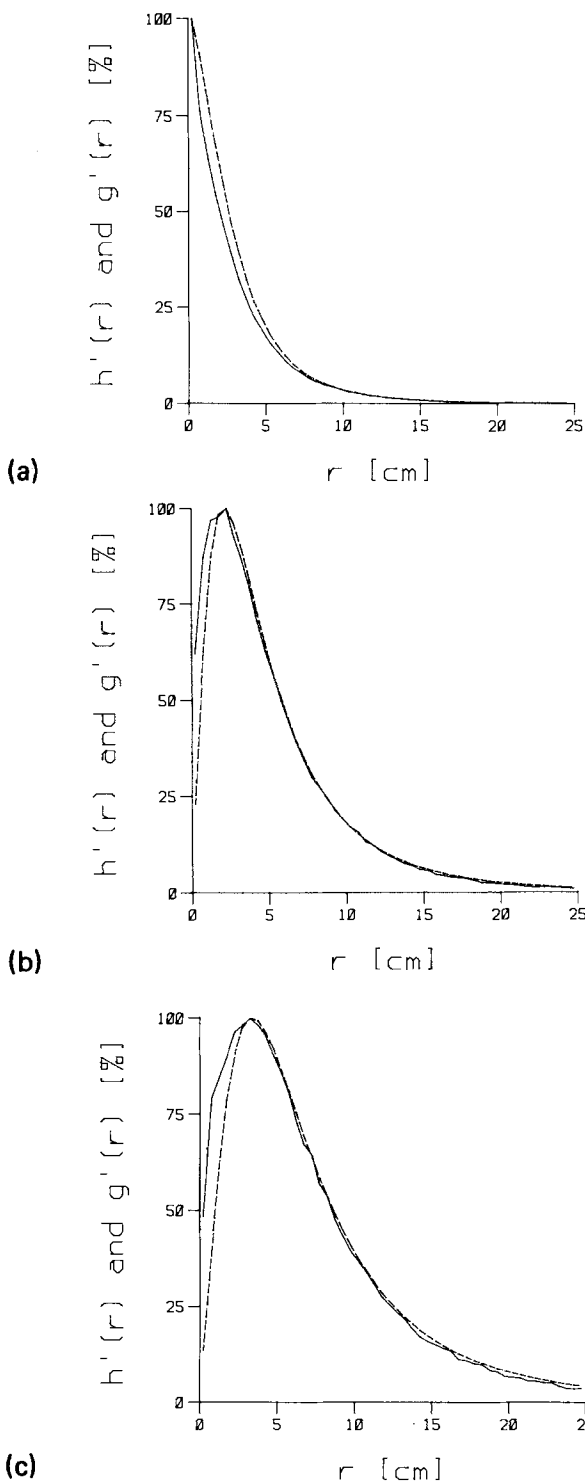


FIG. 2. MC modified PSF $h'(r)$ (solid line) and analytical approximation $g'(r)$ (dashed line). 5-cm object thickness; (a) 0-cm air gap, (b) 2-cm air gap, (c) 4-cm air gap.

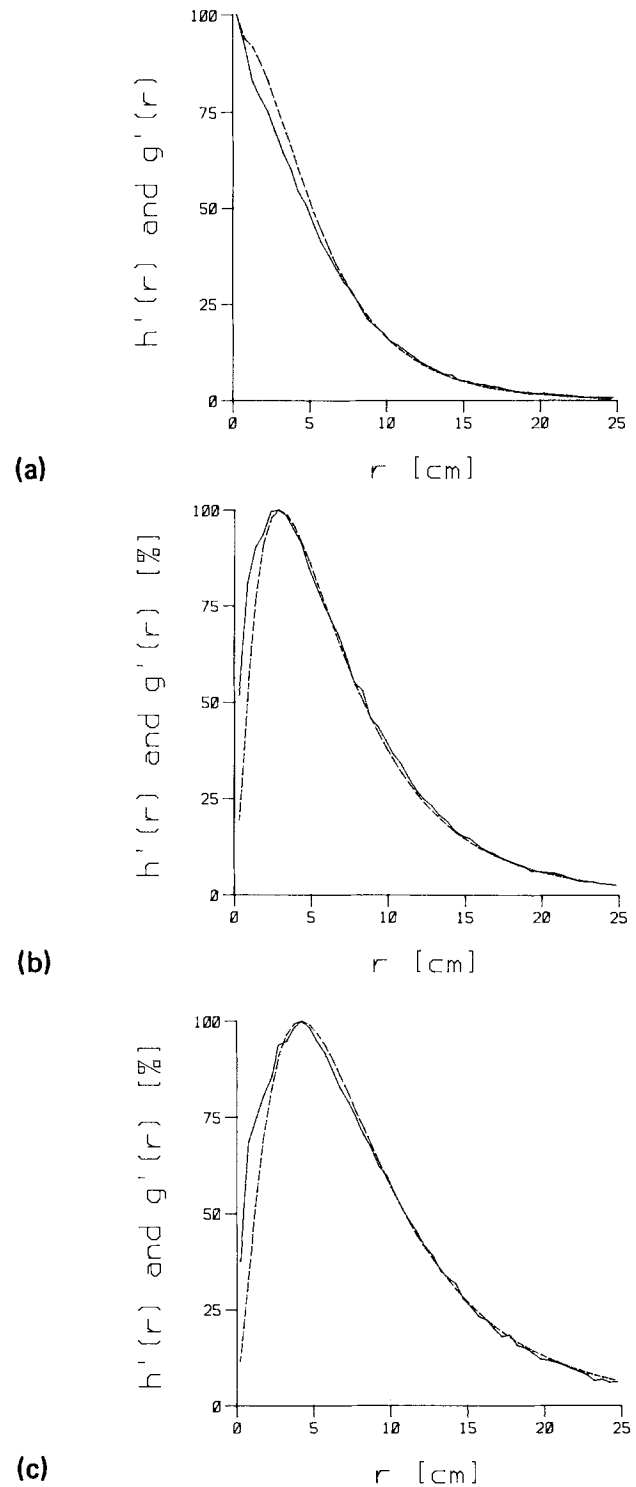


FIG. 3. MC modified PSF $h'(r)$ (solid line) and analytical approximation $g'(r)$ (dashed line). 10-cm object thickness; (a) 0-cm air gap, (b) 2-cm air gap, (c) 4-cm air gap.

listed in Table II for various object thicknesses and x-ray spectra.

IV. DISCUSSION

An excellent relationship between the MC determined PSF $h'(r)$ and the analytically derived function $g'(r)$ is apparent in Figs. 2–5. However, it is also evident that $g'(r)$

generally underestimates $h'(r)$ at small r . This is probably due to the fact that Rayleigh scattering was not considered in the derivation of $g'(r)$, although it is incorporated into the MC simulation [i.e., into $h'(r)$]. Since Rayleigh scattering consists mostly of small angle scattering, not including it in $g'(r)$ implies that $g'(r)$ will underestimate the PSF amplitude at small r . However, this may not be important in terms

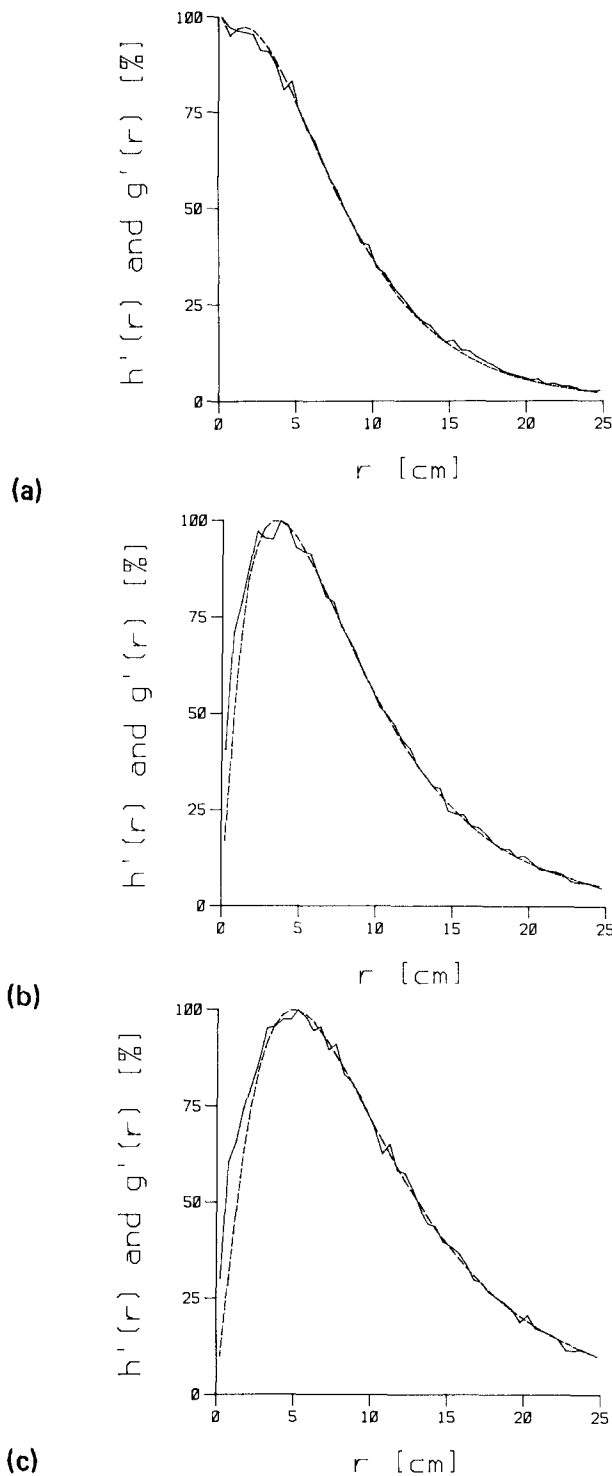


FIG. 4. MC modified PSF $h'(r)$ (solid line) and analytical approximation $g'(r)$ (dashed line). 15-cm object thickness; (a) 0-cm air gap, (b) 2-cm air gap, (c) 4-cm air gap.

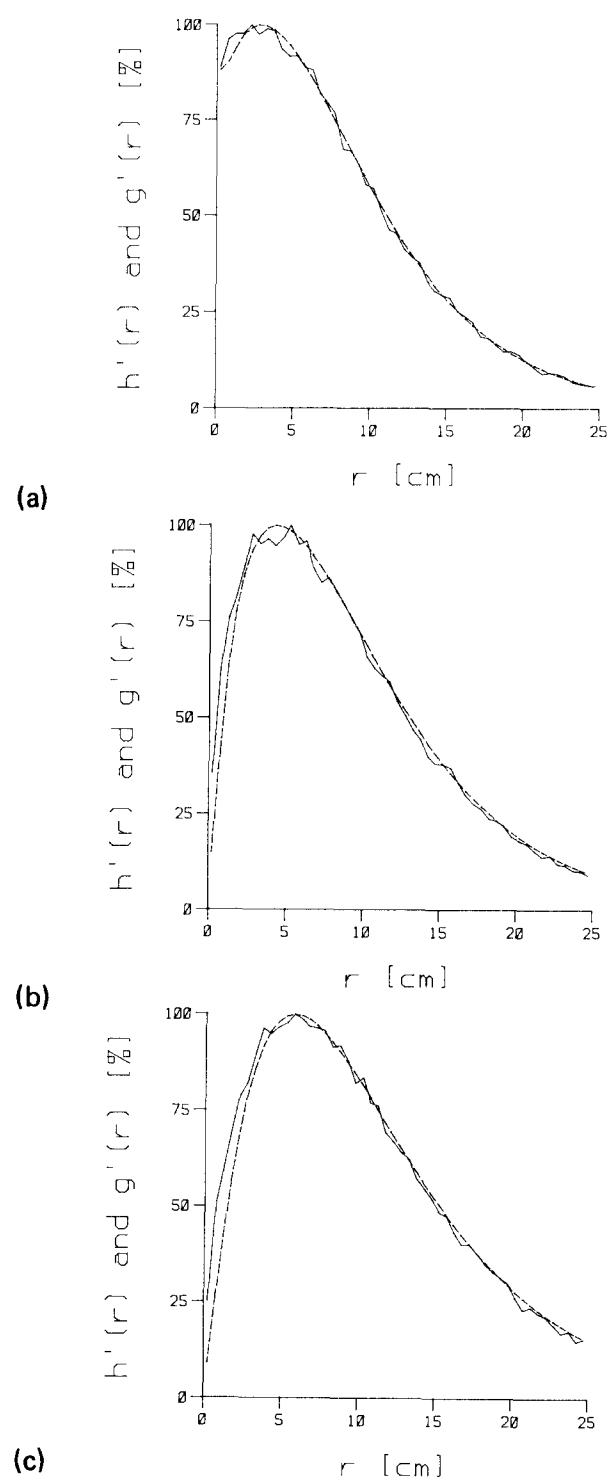


FIG. 5. MC modified PSF $h'(r)$ (solid line) and analytical approximation $g'(r)$ (dashed line). 20-cm object thickness; (a) 0-cm air gap, (b) 2-cm air gap, (c) 4-cm air gap.

of scatter correction, because the majority of the scattered energy is deposited at greater values of r . Furthermore, the contribution of Rayleigh scattering, though not negligible, is small as discussed in the companion paper.

Although $g'(r)$ was derived based on a single scattering model, it does an excellent job at approximating $h'(r)$, which includes multiple scattering effects. This could suggest that

multiple scattering contributes little to the PSF, however evidence shown in the companion paper indicates that this is not the case, especially with thicker objects. Figure 10 in the companion paper illustrates that multiple scattered photons are longer in range, that is, they contribute more to $g'(r)$ at larger values of r , than their singly scattered cousins. In terms of the model used in deriving $g'(r)$, it is noted that the

TABLE I. The values of μ_p and μ_s for different x-ray spectra. μ_p was calculated from the MC experimental data in Ref. 6. μ_s was found using least-squares fitting techniques to the $h'(r)$ distributions measured using MC simulation (Ref. 6). HVL = half-value layer.

kVp	HVL (mm Al)	μ_p cm ⁻¹	μ_s cm ⁻¹
80	1.8	0.2355	0.1399
100	2.3	0.2184	0.1328
120	2.8	0.2079	0.1188

relative range of the function is modulated by the μ_s term. The lateral diffusion of scatter can be increased by lowering μ_s , and can be decreased by increasing μ_s . Therefore, it is plausible that although $g'(r)$ is derived assuming single scattering, the μ_s term behaves in rough analogy like a diffusion coefficient, compensating for the more diffuse multiple scatter. It is noted that since the energy of scattered radiation is less than or equal to that of the primary, the scatter attenuation coefficient should be *greater* than the primary attenuation coefficient, contrary to what is observed empirically (see Table I). Looking at this another way, measured attenuation coefficients decrease as the detection geometry is shifted from good geometry (narrow beam) to poor geometry (broad beam). This is true due to the contribution of scattered photons to the detector. This is what we are observing here. The attenuation coefficient of the singly scattered photons is being reduced due to the contribution of multiply scattered photons in $h'(r)$, the Monte Carlo derived PSF. Recall that unlike the other input parameters, μ_s was determined using least-squares comparison between $g'(r)$ and $h'(r)$. This, in effect, forces the analytic model to conform to the multiple scatter situation through the only degree of freedom available — μ_s . It is worth noting that for the three spectra evaluated (80, 100, and 120 kVp), the ratio μ_s/μ_p is constant (within 3%) at 0.59. If, after further investigation this is found to be generally true, μ_s can be calculated from μ_p and the number of parameters for $g'(r)$ would be reduced from four to three.

TABLE II. The values of SPR_∞ for various object thicknesses and x-ray spectra. SPR_∞ is the ratio between the total scattered energy exiting the bottom of the object, to the total primary energy exiting the object. The object was a homogeneous slab of water. These values were determined by MC simulation, described in a companion paper (Ref. 6).

Object thickness (cm)	SPR_∞		
	80 kVp	100 kVp	120 kVp
5	0.62	0.61	0.60
10	1.36	1.36	1.39
15	2.25	2.26	2.37
20	3.35	3.36	3.62

Equation (9) can be used to calculate the modified PSF $g'(r)$. The PSF $g(r)$ is calculated by multiplying $g'(r)$ by the factor $1/2\pi r$, which accounts for the radial expansion of scatter in the two-dimensional case. Because a singularity occurs in $g(r)$ at $r = 0$, the scatter contribution at $r = 0$ can be accounted for using a dc term. It could be argued that for qualitative purposes, scatter that reaches the image detector at $r = 0$ provides the same information as primary radiation, and thus could be considered as primary.

V. CONCLUSIONS

A point spread function for scattered radiation has been derived from physical principles. The parametric inputs to the equation are physical in nature, two involving the imaging geometry and two related to the x-ray spectra. Though the linear attenuation coefficient for primary radiation μ_p may be found by measurement or derived from tables, the value of μ_s was found empirically by minimizing the squared error between the analytical PSF and the scatter PSF determined using Monte Carlo techniques. It was found for the few spectra analyzed here (three), that to a good approximation $\mu_s/\mu_p = 0.59$. Though the analytical derivation considered only singly scattered photons, it is observed that the analytic PSF $g'(r)$ very closely approximates the multiple scattering PSF $h'(r)$ measured by Monte Carlo techniques. The likely explanation for this is that increasing the value of μ_s increases the attenuation of scatter and therefore reduces its spread. Thus, by reducing μ_s , the PSF can be spread out. This also explains why the empirical value of μ_s is less than μ_p , contrary to what would be expected.

The validity of Eq. (9) has been verified only in the range of parameters described above. While it is anticipated that Eq. (9) is generally applicable, caution should be used when extrapolating the model. Further investigation is warranted in this area.

¹C.-G. Shaw, D. L. Ergun, F. D. Myerowitz, M. S. Van Lysel, C. A. Mistretta, W. C. Zarnstorff, and A. B. Crummy, "A technique of scatter and glare correction for videodensitometric studies in digital subtraction videangiography," *Radiology* **142**, 209 (1982).

²S. W. Smith and R. A. Kruger, "A signal processing model of diagnostic x-ray scatter," *Med. Phys.* **13**, 831 (1986).

³S. Naimuddin, B. Hasegawa, and C. A. Mistretta, "Scatter-glare correction using a convolution algorithm with variable weighting," *Med. Phys.* **14**, 330 (1987).

⁴J. M. Boone, "Scatter correction algorithm for digitally acquired radiographs: Theory and results," *Med. Phys.* **13**, 319 (1986).

⁵J. A. Seibert and J. M. Boone, "X-ray scatter removal by deconvolution," *Med. Phys.* **15**, 567 (1988).

⁶J. M. Boone and J. A. Seibert, "Monte Carlo simulation of the scattered radiation distribution in diagnostic radiology," *Med. Phys.* **15**, 713 (1988) (this issue).

⁷R. D. Evans, *The Atomic Nucleus* (Krieger, Malabar, FL, 1982).